Journal of Microscopy

Journal of Microscopy, Vol. 253, Issue 1 2014, pp. 24–30 doi: 10.1111/jmi.12094
Received 28 May 2013; accepted 27 September 2013

Three-dimensional imaging of whole mouse models: comparing nondestructive X-ray phase-contrast micro-CT with cryotome-based planar epi-illumination imaging

A. TAPFER*, M. BECH*,§, I. ZANETTE*,‖, P. SYMVOULIDIS†,#, S. STANGL‡, G. MULTHOFF‡, M. MOLLS‡, V. NTZIACHRISTOS†,# & F. PFEIFFER*

*Department of Physics and Institute of Medical Engineering, Technische Universität München, Munich, Germany
†Institute for Biological and Medical Imaging, Helmholtz Zentrum München, Neuherberg, Germany
‡Department of Radiation Oncology, Klinikum rechts der Isar, Technische Universität München, Munich, Germany
§Medical Radiation Physics, Clinical Sciences, Lund University, Lund, Sweden
‖European Synchrotron Radiation Facility, Grenoble, France
#Chair for Biological Imaging, Technische Universität München, Munich, Germany

Key words. Computed tomography, planar epi-illumination imaging, X-ray phase contrast.

Summary

In this study, we compare two evolving techniques for obtaining high-resolution 3D anatomical data of a mouse specimen. On the one hand, we investigate cryotome-based planar epi-illumination imaging (cryo-imaging). On the other hand, we examine X-ray phase-contrast micro-computed tomography (micro-CT) using synchrotron radiation. Cryo-imaging is a technique in which an electron multiplying charge coupled camera takes images of a cryo-frozen specimen during the sectioning process. Subsequent image alignment and virtual stacking result in volumetric data. X-ray phase-contrast imaging is based on the minute refraction of X-rays inside the specimen and features higher soft-tissue contrast than conventional, attenuation-based micro-CT. To explore the potential of both techniques for studying whole mouse disease models, one mouse specimen was imaged using both techniques. Obtained data are compared visually and quantitatively, specifically with regard to the visibility of fine anatomical details. Internal structure of the mouse specimen is visible in great detail with both techniques and the study shows in particular that soft-tissue contrast is strongly enhanced in the X-ray phase images compared to the attenuation-based images. This identifies phase-contrast micro-CT as a powerful tool for the study of small animal disease models.

Correspondence to: Arne Tapfer, Physics Department, Technische Universität München, James-Franck-Street, 85748 Garching, Germany. Tel: +49-89-289-12552; fax: +49-289-12548; e-mail: arne.tapfer@tum.de, franz.pfeiffer@tum.de

Introduction

For a profound understanding of diseases, the study of model organisms in biomedical research is an invaluable tool. In this context, histopathology is – in most cases – still the gold standard technique for examining the tissue of interest. This technique is intrinsically 2D and can only be extended to 3D by virtually stacking subsequent slices (Weninger *et al.*, 1998). In order to avoid deformation of tissue and to minimize distortions in the longitudinal direction, a cryotome can be used in combination with an optical camera. In this particular technique, here referred to as cryo-imaging, the camera takes images of cutting surfaces of the frozen specimen in the sectioning process (Wilson *et al.*, 2008; Steyer *et al.*, 2009; Sarantopoulos *et al.*, 2011). Subsequently, these images are aligned and stacked to a pseudo 3D volume. This technique and histopathology in general are labour-intensive, depending on the needed through-plane resolution, and are not well suited for screening of large volumes as required for example in anatomical phenotyping or therapeutic response monitoring. At this point, technical advances in biomedical imaging can offer an alternative.

For high-resolution imaging of whole small animals, most commonly micro-computed tomography (micro-CT) and magnetic resonance imaging are used (Tyszka *et al.*, 2005; Cnudde *et al.*, 2008). Micro-CT features high spatial resolution (on the order of several micrometers), but has difficulty in distinguishing soft tissues (Holdsworth & Thornton, 2002). This limitation can partly be overcome by the injection of a contrast agent, resulting in soft-tissue contrast based on differences in agent uptake and washout dynamics. Magnetic resonance imaging on the other hand, shows high intrinsic

soft-tissue contrast, but is fundamentally limited in spatial resolution (Tyszka *et al.*, 2005). In micro-CT, the limitation in image contrast in soft tissue is due to the limited difference in attenuation properties of light elements. A physically different effect for contrast generation can be utilized with phase-sensitive X-ray imaging techniques. These rely on the phase shift that X-rays undergo when passing through matter (Fitzgerald, 2000). The difference in phase shift – which results in a certain refraction angle – can be made visible as contrast mechanism in a grating interferometer. This technique provides two types of images from one acquisition: conventional attenuation-contrast images and phase-contrast images. Recent studies employing this method have numerously demonstrated improved soft-tissue contrast (Momose *et al.*, 2006; Weitkamp *et al.*, 2008; Jensen *et al.*, 2011; Stampanoni *et al.*, 2011; Stutman *et al.*, 2011; Schulz *et al.*, 2012; Sztrókay *et al.*, 2012; Tapfer *et al.*, 2012). This increased soft-tissue contrast in combination with the capability of high spatial resolution renders phase-contrast CT attractive for high-performance imaging of anatomy.

In the context of small-animal preclinical imaging, the present study investigates two evolving *ex vivo* techniques for high-resolution imaging of mouse anatomy: synchrotron radiation-based phase-contrast CT and cryo-imaging. Specifically, one exemplary healthy mouse specimen was imaged using both techniques and obtained data are compared visually and quantitatively.

Materials and methods

Cryo-imaging

The setup consists of a commercially available rotary cryotome (CM 1950, Leica Microsystems GmbH, Wetzlar, Germany), equipped with a near-infrared sensitive camera (Luca R, Andor Technology plc., Belfast, UK). Because the camera itself is monochromatic, in order to reconstruct the colour image, we use a controllable filter-wheel with an RGB filter-set in front of it. Additional polarizers are used to minimize specular reflections from the ice crystals. Specially developed software controls the sectioning procedure of the cryotome and the image acquisition of the optical system. Essentially, the technique is based on colour images taken directly from the cutting surface of the frozen specimen (episcopic images) during the sectioning process. Figure 1(A) displays the cryo-imaging setup schematically. The generation of a pseudo 3D volume is based on the relative alignment of all images with the help of fiducial markers and subsequent virtual stacking. The sample preparation (embedding and freezing) and data acquisition time (slicing and image capture) for the mouse specimen was approximately 15 h in order to achieve high through-plane resolution of the whole body. The pixel size in-plane was 25 μm, and the slice thickness was $\approx$100 μm. By pausing the slicing procedure, the cryotome can also be used for collecting samples for conventional histopathology. The system is moreover specially designed for multispectral imaging the bio-distribution of fluorescent probes. This feature was, however, not used in the present study as the injection of fluorescent markers requires a living animal. A detailed description of this cryo-imaging system can be found in Sarantopoulos *et al.* (Sarantopoulos *et al.*, 2011).

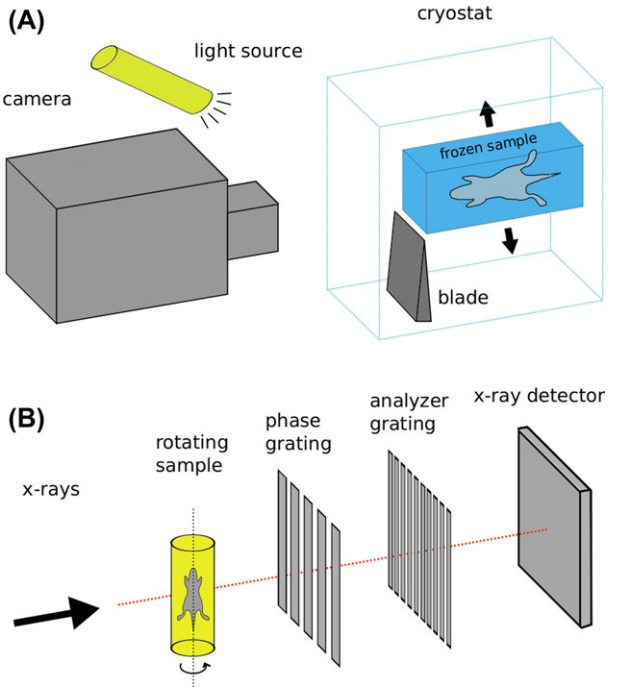

Fig. 1. Schematic view of the cryo-imaging setup (A) and grating-based X-ray phase-contrast CT setup (B).

X-ray grating interferometer

The synchrotron radiation source measurements were carried out at beamline ID19 of the European Synchrotron Radiation Facility in Grenoble, France. Transmission and differential phase images were extracted by a Talbot interferometer and a scintillator/lens-coupled CCD detector (FReLoN) (Weitkamp *et al.*, 2005, 2010). The experimental setup is represented schematically in Fig. 1(B). The inter-grating distance of the phase grating (period 4.79 μm) and the analyser grating (period 2.4 μm) was 408 mm. With an X-ray energy of 35 keV, this corresponds to the 5th fractional Talbot distance, and a phase-shift of π. The monochromator consists of a Si-111 double-crystal monochromator, providing an energy bandwidth of $\Delta E/E \approx 10^{-4}$. For the tomographic scan, 901 projections were acquired over 360 degrees. In the phase-stepping procedure, four images were acquired with an exposure time of 1 s each. As the field-of-view is limited in the longitudinal

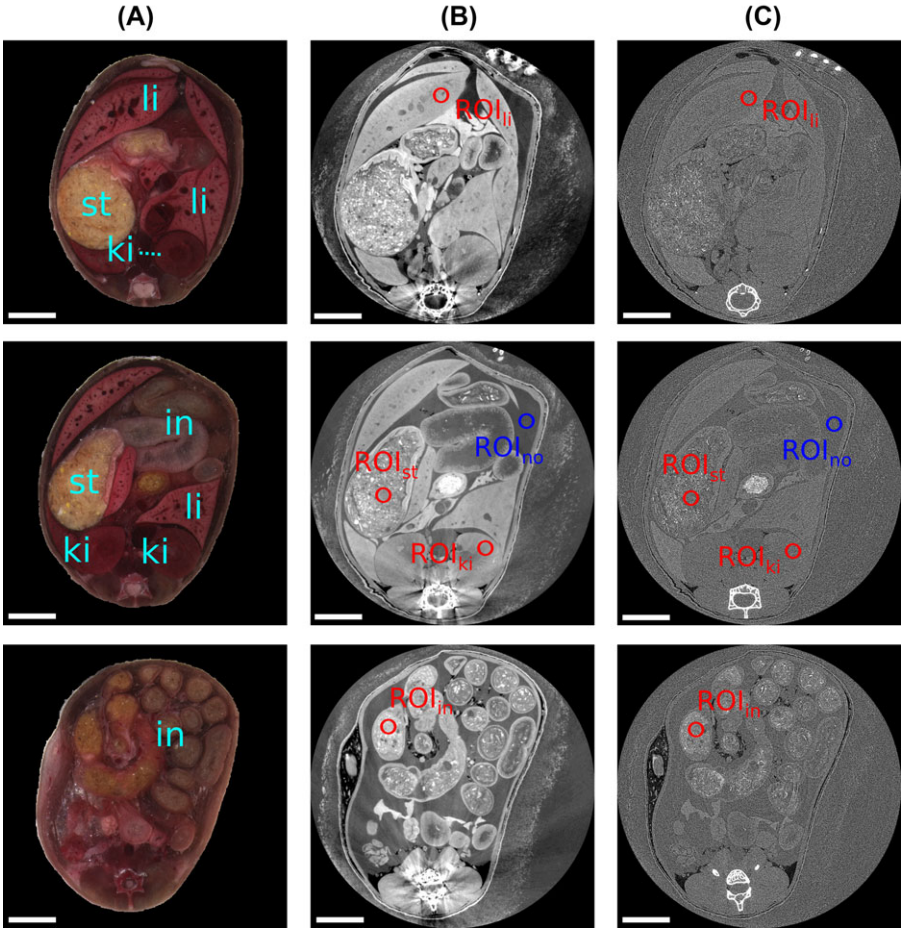

Fig. 2. Transverse slices of all imaging modalities at three different positions: (A) cryo-images, (B) phase-contrast CT images and (C) attenuation-based CT images. In the cryo-images, prominent organs are labelled: stomach (st), liver (li), kidney (ki), intestine (in). For the SNR analysis, the employed ROIs of the corresponding organs are indicated by red circles and the noise ROIs is indicated in blue. All images are displayed on a linear greyscale and are windowed for best visual appearance. The scale bar indicates 5 mm.

direction to 2 cm, two subsequent CT scans were performed, resulting in a total acquisition time of ≈4 h. The effective detector pixel size of 30 μm resulted in an isometric CT volume voxel size of 30 μm. The tomographic reconstruction is quantitative, i.e. the spatial distribution of the linear attenuation coefficient $\mu(x, y)$ and decrement of the refractive index $\delta(x, y)$ is accessible (Weitkamp *et al.*, 2005; Herzen *et al.*, 2009; Qi *et al.*, 2010; Tapfer *et al.*, 2011). The latter quantity directly maps electron density.

Image analysis

The data sets of both techniques were aligned by hand using rigid transformations. Due to the nearly identical specimen positioning during X-ray acquisition and subsequent cryo-freezing of the entire mouse, misalignment of both data sets was minimal and sophisticated software registration as used for example by Müller et al. (Müller *et al.*, 2012) was not necessary. The comparison of visibility of different tissues for both methods is done by visual inspection. For the X-ray data, attenuation and phase images were additionally compared quantitatively. Please note that attenuation and phase images are intrinsically perfectly registered as both originate from one common data set. For the quantitative comparison of both images, regions-of-interest (ROI) within several organs were selected and the signal-to-noise ratio (SNR) was determined. When determining the SNR using the standard deviation to probe noise, one aspect has to be considered: the standard deviation in a ROI reflects two opposing effects, namely image noise and tissue heterogeneity. Image noise should of course be considered in the SNR, unlike tissue heterogeneity that – if present within the ROI – also increases the standard deviation and consequently appears falsely as additional noise. To overcome this problem, the noise estimate in this analysis was not determined from the organ ROI itself, but rather using a dedicated noise ROI that covers a homogeneous image region. Based on the mean value of the ROI of a specific organ i, M_i, and the standard deviation σ from the noise ROI, the SNR was

calculated according to

$$\mathrm{SNR_i} = \frac{M_\mathrm{i}}{\sigma}. \quad (1)$$

The uncertainty of the SNR (σ_{SNR}) was determined by applying standard error (SE) propagation to the equation of the SNR (Eq. (1)). The required uncertainties are the SE of each mean value ($\mathrm{SE_{mean}} = \frac{\sigma}{\sqrt{N}}$) and the SE of the noise estimate ($\mathrm{SE}_\sigma = \frac{\sigma}{\sqrt{2N}}$) (Press *et al.*, 2007). N denotes the number of voxels in the corresponding ROI.

Results

In Fig. 2, three transverse views of the abdomen are shown: (A) cryo-images, (B) phase images, (C) attenuation images. The transverse slice in the top row is located inferior to the lung, the middle row's slice covers both kidneys, and the bottom row is superior to the hip. Prominent organs that can clearly be identified are the stomach (st), several lobes of the liver (li), kidney (ki) and intestines (in). All of these are highlighted only in the cryo-images. When comparing the cryo- and X-ray images, the good correlation becomes apparent. Only few slight deformations in shape are present. Moreover, please note that the cryo-images are not strictly surface images as the light penetrates noticeably the surface layer of tissue. In the phase images, streaking artefacts are present, which originate from the strongly phase-shifting bones. Both in origin and appearance, these streaking artefacts are comparable to streaking artefacts originating from metal implants in clinical CT.

When regarding the cryo-images, all organs can be easily identified as expected. Here, the difference in colour significantly improves discernibility of organs. Also in the phase image, all organs can be clearly identified. For the attenuation image, the recognizability of organs is markedly compromised. In particular, soft-tissue contrast is strongly reduced and only bone tissue generates a strong contrast. When examining smaller structures – i.e. fine anatomical details within the mentioned organs – a similar observation can be made. As an example, the liver and the kidney of the top row are considered. In the cryo-image, the blood vessel network is clearly visible within the liver (appearing darker). Many of these blood vessels are also visible in the phase image, however less clearly. In the attenuation image on the other hand, the liver – as most other organs – does almost not exhibit any internal structure. Similarly, internal structure of the kidney is visible in the cryo- and phase image, unlike in the attenuation image.

As the pixel size is very similar in the cryo-images (25 μm) and the X-ray images (30 μm), the reason for the described visual observations is not spatial resolution but rather image contrast. More precisely, the crucial difference lies within the SNR, which is analysed in the following. Due to the colour information of the cryo-images, a direct comparison with the greyscale X-ray images is not straightforward, and the following SNR analysis is performed only for the attenuation and phase images. The analysis is based on ROIs, which cover several organs and a separate ROI that is used to probe noise. The organ ROIs are indicated by red circles with the corresponding organ depicted as index. The noise ROI is shown in both the phase and the attenuation image as blue circle ($\mathrm{ROI_{no}}$). Table 1 lists the SNR values that were determined in this manner. These quantitative values confirm the described visual impression, with approximately seven times larger SNRs in the phase images.

Table 1. Signal-to-noise ratios in attenuation and phase images for selected tissues are listed.

	Attenuation	Phase
Liver	15.2 ± 0.3	107 ± 2
Stomach	15.2 ± 0.3	108 ± 2
Kidney	15.1 ± 0.3	107 ± 2
Intestine	16.0 ± 0.3	117 ± 2

Figure 3 displays coronal slices of the cryo-volume (A), the phase- (B) and attenuation data (C). Good correlation between the cryo-image and the X-ray images is also given in this case. However, it becomes apparent that the cryo-based technique naturally performs worse in the longitudinal direction: horizontally oriented distortions are visible, which are caused by the virtual stacking. The X-ray data on the other hand is truly 3D and any slice orientation is accessible. Also in the phase image few horizontally oriented stripes are visible. These are due to the differential nature of the phase signal. Additionally, these are overlaid by the previously mentioned bone-induced streaking artefacts.

Discussion

Present preclinical research on small animals aims at fundamentally understanding various pathologies. Moreover, anatomical phenotyping is of great interest, especially due to the ever increasing access to genetically engineered animals. For these and potentially also other applications that require high spatial resolution 3D data with pronounced soft-tissue visibility, phase-contrast CT and cryo-imaging have shown great potential. In the following the advantages and limitations of both techniques are considered briefly.

Cryo-imaging, which is compatible with acquiring conventional histological sections, can be combined with staining for gene and protein expression. The experimental setup does moreover have the capability to image the bio-distribution of fluorescent probes, which allows for functional imaging. The technique is for these reasons very well suited as a validation technique for novel nondestructive imaging modalities and has, for example, been used in combination with multispectral optoacoustic tomography and fluorescence molecular tomography (Ale *et al.*, 2012; Herzog *et al.*, 2012; Taruttis

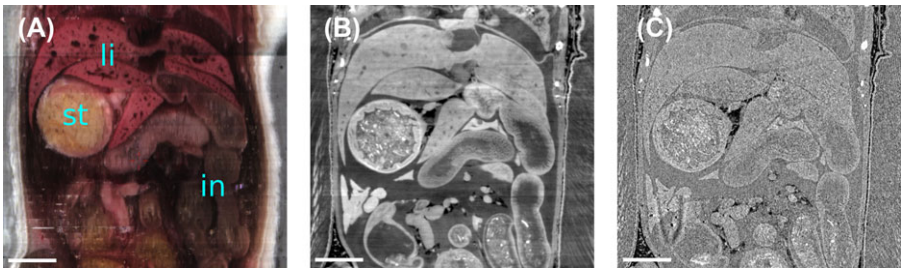

Fig. 3. Coronal views of all imaging modalities: (A) cryo-image, (B) phase image, (C) attenuation image. The stomach (st), liver (li) and intestines (in) are labelled. All images are displayed on a linear greyscale and are windowed for best visual appearance. The scale bar indicates 5 mm.

Table 2. Overview of properties of both reviewed modalities, cryo-imaging and phase-contrast CT.

	Cryo-imaging	Phase-contrast CT
Pixel size (μm)		
In-plane	25	30
Through-plane	75–125	30
Acquisition time (h)	≈15	≈ 4
Volume format	Pseudo 3D	Truly 3D
Sample preparation /handling	Cryo-sectioning (destructive)	Fixation (nondestructive)
Other features	Histological staining	Two complementary contrasts
	Fluorescent bio-markers	Quantitative (μ and δ)

et al., 2013). The use of combinations of narrow-band filters can also further increase the contrast of intrinsic tissue chromophores, such as hemoglobin. The range of applications is of course limited due to the destructive nature and the expense in labour involving sample preparation, the physical slicing, photographing and post-alignment. In the case that a 3D volume is generated, additional software post-processing is necessary and slight distortions in the longitudinal direction can hardly be avoided with the setup used. Using a different cryotome, the process can be fully automated, decreasing the workload and the user-depended acquisition artefacts, like misalignments. The addition of xy-stages to scan the sample with a microscopic lens can further increase the resolution, by tiling multiple images for each plane.

Tomographic imaging in general allows for a higher and more user-friendly throughput, is nondestructive and results in truly 3D data volumes, with isotropic spatial resolution in all three orthogonal directions. Also samples that are difficult to slice can be handled and the intrinsic digital nature of tomographic data allows for straightforward software post-processing, such as for example volume quantification or segmentation.

In this context, Table 2 summarizes relevant properties and technical parameters of both reviewed methods.

Technically, a higher spatial resolution is easily achievable for both reviewed techniques by using different camera optics or a different X-ray detector respectively. In particular, for the phase images, it has been reported in the literature that a smaller pixel size is beneficial for the SNR (Chen *et al.*, 2011; Engel *et al.*, 2011; Köhler *et al.*, 2011).

Concerning the X-ray data acquisition time, there is significant room for optimization. This relates to both the experimental imaging setup and the data collection scheme. With respect to the experimental setup, the exposure time can be reduced by several orders of magnitude when increasing the photon flux by using a larger energy bandwidth in the few percent range, so called 'pink beam'. As the grating interferometer is proven to be highly achromatic, the imaging performance would not be degraded (Engelhardt *et al.*, 2008). With regard to data acquisition, the significantly shorter acquisition time would allow for continuous-rotation CT scans, or rather several continuous-rotation CT scans for each grating position. Alternatively, acquisition time can be reduced by combining phase stepping and sample rotation as recently reported by Zanette *et al.* (2012). Altogether, CT scans with comparable image quality are feasible with acquisition times on the order of half an hour or less.

With respect to routine investigations, for which a synchrotron is not ideally suited due to limited access, also conventional laboratory X-ray tubes can be employed for phase-contrast measurements, when an additional source grating is used to provide sufficient spatial coherence (Pfeiffer *et al.*, 2006). If the focus is on high-spatial resolution, the interferometer can be operated with a microfocus X-ray tube, as commonly done in conventional absorption-based imaging. When the grating interferometer is operated with an X-ray tube rather than with monochromatized synchrotron radiation, image quality is reduced due to two effects: the photon flux is lower (affecting statistical image noise) and the polychromatic nature of the X-rays reduces the performance of the interferometer and moreover gives rise to beam-hardening artefacts. Nevertheless, increased soft-tissue contrast has been demonstrated in several tube-based biomedical CT imaging experiments (Bech *et al.*, 2009; Donath *et al.*, 2010; Grandl *et al.*, 2013). A comparison of synchrotron and tube-based phase-contrast imaging for the case of a mouse tumor model can be found in Tapfer *et al.* (2013).

Other noninvasive imaging techniques with dedicated instruments for small animals besides magnetic resonance imaging include single-photon emission computed tomography, positron emission tomography and several optical imaging techniques. Compared to X-ray-based techniques, spatial resolution is strongly inferior in the emission techniques (single-photon emission computed tomography and positron emission tomography) and also magnetic resonance imaging is fundamentally limited in spatial resolution due to molecular diffusion, T2 relaxation and magnetic field inhomogeneities (Callaghan, 1993). For optical techniques, the main limitation is penetration depth (Ntziachristos, 2010). Here, grating-based phase-contrast CT offers the complementarity of two contrasts, combining high soft-tissue contrast with a good representation of the skeleton at high spatial resolution.

Conclusion

In this study, the imaging performance of cryo-imaging and grating-based phase-contrast CT, with phase- and attenuation-contrast images, was investigated on one healthy mouse specimen. In particular, the potential for high-resolution anatomical imaging was assessed. Besides a visual comparison of all imaging modalities, especially the attenuation and phase images were compared quantitatively, based on a SNR analysis of several organs in the abdomen. Here, it was demonstrated that soft-tissue contrast is strongly improved in the x-ray phase data compared to the x-ray absorption data.

The vast differences of both techniques result in different advantages and limitations. Cryo-imaging is compatible with conventional histology – allowing for staining of gene and protein expression – and it is very well suited as a validation technique. However, it is destructive and labor-intense. Grating-based phase-contrast imaging is nondestructive, allows for a higher throughput, and delivers truly volumetric data with two complementary image contrasts, yet images may suffer from bone artefacts.

Acknowledgements

We thankfully acknowledge help from T. Weitkamp during the synchrotron-based experiment. The project was partially supported by the ESRF (proposal MI983) through beamtime allocation. Moreover, we gratefully acknowledge A. Sarantopoulos and G. Themelis for their help with the cryo-imaging data acquisitions and useful discussions. A.T., M.B., I.Z. and F.P. acknowledge financial support through the DFG Cluster of Excellence Munich Centre for Advanced Photonics (MAP), the DFG Gottfried Wilhelm Leibniz program and the European Research Council (ERC, FP7, StG 240142). A.T. acknowledges the graduate school of Technische Universität München (TUM Graduate School). Gabriele Multhoff's laboratory is supported, in part, by the Helmholtz Zentrum München (Clinical Cooperation Group – 'Innate Immunity in Tumor Biology'), the Deutsche Forschungsgemeinschaft (SFB824/1; DFG Cluster of Excellence, Munich Centre for Advanced Photonics, MAP), the Bundesministerium für Forschung und Technologie (BMBF BioChance plus, 0313686A; BMBF MOBITUM, 01EZ0826; BMBF Kompetenzverbund Strahlenforschung, 03NUK007E; BMBF Innovative Therapies, 01GU0823; BMBF m4 Spitzencluster, 01EX1021C).

References

Ale, A., Ermolayev, V., Herzog, E., Cohrs, C., de Angelis, M.H. & Ntziachristos, V. (2012) FMT-XCT: *in vivo* animal studies with hybrid fluorescence molecular tomography-X-ray computed tomography. *Nat. Methods* **9**, 615–620.

Bech, M., Jensen, T., Feidenhans'l, R., Bunk, O., David, C. & Pfeiffer, F. (2009) Soft-tissue phase-contrast tomography with an x-ray tube source. *Phys. Med. Biol.* **54**, 2747–2753.

Callaghan, P. (1993) *Principles of Nuclear Magnetic Resonance Microscopy*. Clarendon Press, Oxford.

Chen, G., Zambelli, J., Li, K., Bevins, N. & Qi, Z. (2011) Scaling law for noise variance and spatial resolution in differential phase contrast computed tomography. *Medical Phys.* **38**, 584–588.

Cnudde, V., Masschaele, B., De Cock, H.E.V., *et al.* (2008) Virtual histology by means of high-resolution X-ray CT. *J. Microsc.* **232**, 476–485.

Donath, T., Pfeiffer, F., Bunk, O., Grünzweig, C., Hempel, E., Popescu, S., Vock, P. & David, C. (2010) Toward clinical X-ray phase-contrast CT: demonstration of enhanced soft-tissue contrast in human specimen. *Invest. Radiol.* **45**, 445–452.

Engel, K.J., Geller, D., Köhler, T., Martens, G., Schusser, S., Vogtmeier, G. & Rössl, E. (2011) Contrast-to-noise in X-ray differential phase contrast imaging. *Nucl. Instrum. Methods Phys. Res. A* **648**, S202–S207.

Engelhardt, M., Kottler, C., Bunk, O., David, C., Schroer, C., Baumann, J., Schuster, M. & Pfeiffer, F. (2008) The fractional Talbot effect in differential x-ray phase-contrast imaging for extended and polychromatic x-ray sources. *J. Microsc.* **232**, 145–157.

Fitzgerald, R. (2000) Phase-sensitive x-ray imaging. *Phys. Today* **53**, 23–26.

Grandl, S., Willner, M., Herzen, J., *et al.* (2013) Evaluation of phase-contrast CT of breast tissue at conventional X-ray sources – presentation of selected findings. *Zeitschrift für medizinische Physik* **23**, 212–221.

Herzen, J., Donath, T., Pfeiffer, F., Bunk, O., Padeste, C., Beckmann, F., Schreyer, A. & David, C. (2009) Quantitative phase-contrast tomography of a liquid phantom using a conventional x-ray tube source. *Opt. Express* **17**, 622–628.

Herzog, E., Taruttis, A., Beziere, N., Lutich, A.A., Razansky, D. & Ntziachristos, V. (2012) Optical imaging of cancer heterogeneity with multispectral optoacoustic tomography. *Radiology* **263**, 461–468.

Holdsworth, D.W. & Thornton, M.M. (2002) Micro-CT in small animal and specimen imaging. *Trends Biotechnol.* **20**, S34–S39.

Jensen, T.H., Böttiger, A., Bech, M., *et al.* (2011) X-ray phase-contrast tomography of porcine fat and rind. *Meat Sci.* **88**, 379–383.

Köhler, T., Engel, K.J. & Rössl, E. (2011) Noise properties of grating-based x-ray phase contrast computed tomography. *Med. Phys.* **38**, S106–S116.

Momose, A., Yashiro, W., Takeda, Y., Suzuki, Y. & Hattori, T. (2006) Phase tomography by x-ray Talbot interferometry for biological imaging. *Jpn J. Appl. Phys.* **45**, 5254–5262.

Müller, B., Deyhle, H., Lang, S., Schulz, G., Bormann, T., Fierz, F.C. & Hieber, S.E. (2012) Three-dimensional registration of tomography data for quantification in biomaterials science. *Int. J. Mater. Res.* **103**, 242–249.

Ntziachristos, V. (2010) Going deeper than microscopy: the optical imaging frontier in biology. *Nat. Methods* **7**, 603–614.

Pfeiffer, F., Weitkamp, T., Bunk, O. & David, C. (2006) Phase retrieval and differential phase-contrast imaging with low-brilliance X-ray sources. *Nat. Phys.* **2**, 258–261.

Press, W.H., Teukolsky, S.A., Vetterling, W.T. & Flannery, B.P. (2007) *Numerical Recipes: The Art of Scientific Computing*. 3rd edn., vol. **1**. Cambridge University Press, Cambridge.

Qi, Z., Zambelli, J., Bevins, N. & Chen, G. (2010) Quantitative imaging of electron density and effective atomic number using phase contrast CT. *Phys. Med. Biol.* **55**, 2669.

Sarantopoulos, A., Themelis, G. & Ntziachristos, V. (2011) Imaging the bio-distribution of fluorescent probes using multispectral epi-illumination cryoslicing imaging. *Mole. Imaging Biol.* **13**, 874–885.

Schulz, G., Waschkies, C., Pfeiffer, F., Zanette, I., Weitkamp, T., David, C. & Müller, B. (2012) Multimodal imaging of human cerebellum – merging X-ray phase microtomography, magnetic resonance microscopy and histology. *Sci. Rep.* **2**, 826.

Stampanoni, M., Wang, Z., Thüring, T., *et al.* (2011) The first analysis and clinical evaluation of native breast tissue using differential phase-contrast mammography. *Invest. Radiol.* **46**, 801–806.

Steyer, G.J., Roy, D., Salvado, O., Stone, M.E. & Wilson, D.L. (2009) Cryo-imaging of fluorescently-labeled single cells in a mouse. *Proc. Soc. Photo-Opt. Instrum. Eng.* **7262**, 72620W–72620W8.

Stutman, D., Beck, T.J., Carrino, J.A. & Bingham, C.O. (2011) Talbot phase-contrast x-ray imaging for the small joints of the hand. *Phys. Med. Biol.* **56**, 5697–5720.

Sztrókay, A., Herzen, J., Auweter, S.D., *et al.* (2012) Assessment of grating-based X-ray phase-contrast CT for differentiation of invasive ductal carcinoma and ductal carcinoma in situ in an experimental ex vivo set-up. *Eur. Radiol.* **23**, 381–387.

Tapfer, A., Bech, M., Pauwels, B., *et al.* (2011) Development of a prototype gantry system for preclinical x-ray phase-contrast computed tomography. *Med. Phys.* **38**, 5910–5915.

Tapfer, A., Bech, M., Velroyen, A., *et al.* (2012) Experimental results from a preclinical X-ray phase-contrast CT scanner. *Proc. Natl. Acad. Sci. USA* **109**, 15691–15696.

Tapfer, A., Braren, R., Bech, M., *et al.* (2013) X-ray phase-contrast CT of a pancreatic ductal adenocarcinoma mouse model. *PLoS ONE* **8**, e58439.

Taruttis, A., Wildgruber, M., Kosanke, K., *et al.* (2013) Multispectral optoacoustic tomography of myocardial infarction. *Photoacoustics* **1**, e3–e8.

Tyszka, J.M., Fraser, S.E. & Jacobs, R.E. (2005) Magnetic resonance microscopy: recent advances and applications. *Curr. Opin. Biotechnol.* **16**, 93–99.

Weitkamp, T., David, C., Bunk, O., Bruder, J., Cloetens, P. & Pfeiffer, F. (2008) X-ray phase radiography and tomography of soft tissue using grating interferometry. *Eur. J. Radiol.* **68**, S13–S17.

Weitkamp, T., Diaz, A., David, C., Pfeiffer, F., Stampanoni, M., Cloetens, P. & Ziegler, E. (2005) X-ray phase imaging with a grating interferometer. *Opt. Express* **13**, 6296–6304.

Weitkamp, T., Zanette, I., David, C., *et al.* (2010) Recent developments in x-ray Talbot interferometry at ESRF-ID19. In *SPIE Conf. Proc.*, ed. S.R. Stock, vol. **7804**, 780406–780410.

Weninger, W.J., Meng, S., Streicher, J. & Müller, G.B. (1998) A new episcopic method for rapid 3-D reconstruction: applications in anatomy and embryology. *Anat. Embryol.* **197**, 341–348.

Wilson, D., Roy, D., Steyer, G., Gargesha, M., Stone, M. & McKinley, E. (2008) Whole mouse cryo-imaging. *Proc. Soc. Photo-Opt. Instrum. Eng.* **6916**, 69161I–69161I9.

Zanette, I., Bech, M., Rack, A., Le Duc, G., Tafforeau, P., David, C., Mohr, J., Pfeiffer, F. & Weitkamp, T. (2012) Trimodal low-dose X-ray tomography. *Proc. Natl. Acad. Sci. USA* **109**, 10199–10204.